Evaluation of Dynamic Features of *Escherichia coli* 16S Ribosomal RNA in Homogeneous Physiological Solution

Takashi Sakamoto,* Atsushi Mahara,† Koichi Yamagata,‡ Reiko Iwase,§ Tetsuji Yamaoka,† and Akira Murakami*

*Department of Polymer Science and Engineering, Kyoto Institute of Technology, Sakyo-ku, Kyoto, Japan; †Department of Biomedical Engineering, Advanced Medical Engineering Center, National Cardiovascular Center Research Institute, Suita, Osaka, Japan; ‡BMI Laboratory, Central Research Laboratories, Sysmex Corporation, Kobe, Hyogo, Japan; and §Department of Bioscience, Teikyo University of Science and Technology, Uenohara, Yamanashi, Japan

ABSTRACT There is no methodology for the estimation of the dynamic features of large-molecular-weight RNAs in homogeneous physiological media. In this report, a luminescence anisotropy-based method using a long-lifetime luminescent oligonucleotide probe for the estimation of the dynamic features of large-molecular-weight RNA is described. As a luminescent probe, Ru(II) complex-labeled oligonucleotides, which have a complementary sequence to the single-stranded regions of *Escherichia coli* 16S rRNA, were synthesized. After the hybridization of the probe to single-stranded regions of 16S rRNA, the segmental motions of the regions were evaluated by time-resolved luminescence anisotropy analysis. In 16S rRNA, the L2 site (323–332 nt) was found to be the most flexible among the seven sites chosen. From a comparison between the hybridization kinetics of oligonucleotides to these single-stranded regions and the rotational correlation times, it was suggested that the flexibility of the single-stranded region was closely correlated with the hybridization kinetics. Furthermore, results of the luminescence lifetime measurement and luminescence quenching experiments suggested that the highly flexible region was located on the surface of the 16S rRNA and that the less flexible region was located in the depths of 16S rRNA.

INTRODUCTION

The recent development of methodologies for the structural study of biomolecules enables researchers to predict interactions between biomolecules and to design effective inhibitors for particular biomolecules. Especially in structural studies of proteins, information on the correlation between function and structure has largely contributed to structure-based drug discoveries. Contrarily, the structural studies of RNA are limited to some extent due to its enormous diversity. Recently, bacterial 30S and 50S ribosomal subunits were crystallized and their three-dimensional structures were reported (1,2). As for the 50S ribosomal subunit, the relationship between the structure and the function has been revealed (3). However, these are rare examples and it will take more time to determine the three-dimensional structures of other RNAs. Furthermore, structural dynamics is an important issue for further understanding the functions of biomolecules. The dynamic features of biomolecules should be taken into consideration when analyzing the interaction between biomolecules. X-ray crystallography, which is mainly used for the determination of the structure of biomolecules (4,5), can only evaluate a static structure. To evaluate dynamic features of RNA, the development of sophisticated methods other than crystallography might contribute to the structure-based discovery of RNA-regulating molecules such as small-interference RNAs and antisense oligonucleotides. As methods for evaluating the dynamic features of biomolecules, NMR (6,7), electron paramagnetic resonance (EPR) (8,9), and fluorescence-based methods (10,11) have been reported. Nuclear spin relaxation measurement based on NMR spectroscopy using ^{1}H, ^{13}C, ^{15}N, and ^{31}P has been frequently used for the determination of the intramolecular flexibility of tRNA (12,13) and small proteins (14). The distinguishing feature of NMR is, in principle, that the method requires no specific labeling of biomolecules. However, the signal resolution limits the applicable molecular-weight range of the specimen ($<$20 kDa in molecular mass). EPR measurement (15) requires the spin-labeling of biomolecules at the designated site. Furthermore, NMR or EPR spectroscopy requires a large quantity of the specimen (several milligrams in weight); therefore, the applicability of these methods is limited to biomolecules that can be easily obtained. As another method to evaluate the dynamic features of biomolecules, fluorescence-based methods have been reported. Tuschl et al. delineated the conformational dynamics of hammerhead ribozyme by fluorescence resonance energy transfer analysis (10). This method is certainly useful for evaluating the structural dynamics of biomolecules. As for proteins, fluorescence anisotropy was measured using internal chromophores such as tryptophan, and the rotational correlation time (θ) derived from fluorescence anisotropy delineated the rotational motion around the tryptophan residue (16). This method has not been applied to evaluate the dynamic features of highly folded RNA.

In this study, we paid attention to the segmental motion of a single strand of folded RNA to estimate the dynamic structure of large-molecular-weight RNA ($>$100 kDa). We adopted time-resolved luminescence anisotropy analysis using a luminescent DNA probe to evaluate the segmental motions

Submitted March 7, 2005, and accepted for publication August 22, 2005.

Address reprint requests to Akira Murakami, E-mail: akiram@kit.ac.jp.

0006-3495/05/12/4122/07 $2.00

doi: 10.1529/biophysj.105.062455

of the single-stranded regions of the folded RNA. *Escherichia coli* 16S rRNA (16S rRNA; ~500 kDa) was used as the model folded RNA. In time-resolved luminescence anisotropy analysis, the rotational motion of the molecule is evaluated by θ. It is theoretically estimated that the θ value of single-stranded regions of 16S rRNA ranges from 100 ns to a few μs. Therefore, long-lifetime luminescence probes (10 ns to 1 μs) are required to evaluate large θ values (100 ns to 10 μs) (17). In this study, as a long-lifetime luminescent material, we adopted the Tris-1,10-phenanthroline Ru(II) complex with a lifetime in the range of 500 ns to 1 μs (18). The Ru(II) complex was conjugated to the oligodeoxyribonucleotides (Ru-probes), and the Ru-probes were successfully used as probes for the evaluation of the segmental motions of single-stranded regions of 16S rRNA.

EXPERIMENTAL

Chemicals

Ruthenium trichloride ($RuCl_3$) and organic solvents were purchased from Wako Chemicals (Osaka, Japan). 1,10-Phenanthroline was purchased from Aldrich Chemical (St. Louis, MO). 5-Nitro-1,10-phenanthroline was purchased from Tokyo Kasei Kogyo (Tokyo, Japan). Reagents for the oligonucleotide synthesis were purchased from Glen Research (Sterling, VA). A mixture of 16S and 23S rRNAs was purchased from Roche (Basel, Switzerland) and used without further purification.

Synthesis of Ru(II) complex-labeled oligodeoxyribonucleotide

The Ru(II) complex-labeled oligodeoxyribonucleotides were synthesized according to Scheme 1.

Fmoc-6-aminohexanoic acid

According to the general F-moc protection procedure (19), 6-aminohexanoic acid (0.79 g, 6 mmols) and triethylamine (0.84 ml, 6 mmols) were dissolved in MilliQ water (3 ml), and Fmoc-*N*-hydroxysuccineimide solution (1.96 g, 5.8 mmols/acetonitrile (6 ml)) was added to the solution. The reaction solution was adjusted to pH 8.5–9.0 and then stirred at room temperature. After 2 h, the solution was filtered, and 1.5 N HCl aqueous solution (~20 ml) was added to the filtrate. The resulting white precipitate was collected by filtration, and the precipitate was washed with MilliQ water, with a yield of 1.64 g (80%).

5-(Fmoc-6-aminohexaneamide)-1,10-phenanthroline

5-Amino-1,10-phenanthroline was synthesized according to a reported procedure (20). Fmoc-6-aminohexanoic anhydride was obtained from the condensation reaction of Fmoc-6-aminohexanoic acid (1.98 g, 5.6 mmols) with *N*,*N*′-dicyclohexylcarbodiimide (0.58 g, 2.8 mmols) in dry dichloromethane. Fmoc-6-aminohexanoic anhydride was mixed with 5-amino-1,10-phenanthroline (0.17 g, 0.9 mmols) in dry dichloromethane/acetonitrile (1:1 v/v) and stirred at room temperature for 160 h. The resulting yellow-white precipitate was collected by filtration, washed with dichloromethane/acetonitrile 1:1 (v/v), and dried in vacuo, for a yield of 0.36 g (68%).

Bis-(1,10-phenanthroline) 5-(6-aminohexaneamide)-1,10-phenanthroline Ru(II) dihexafluorophosphate

Dichloro-bis-1,10-phenanthroline Ru(II) dehydrate ($Ru(phen)_2Cl_2$) was synthesized according to the reported procedure (21). The heteroligand Ru(II) complex was synthesized according to the reported procedure (22) with some modifications. 5-(Fmoc-6-aminohexaneamide)-1,10-phenanthroline (0.053 g, 0.1 mmols) and $Ru(phen)_2Cl_2$ (0.057 g, 0.1 mmols) were dissolved in H_2O/EtOH (1:2 (v/v), 3 ml), and the solution was refluxed for 6 h. The reaction solution was evaporated to dryness, and the residue was dissolved in MilliQ water (16 ml). The unreacted 5-(Fmoc-6-aminohexaneamide)-1,10-phenanthroline and $Ru(phen)_2Cl_2$ were removed by

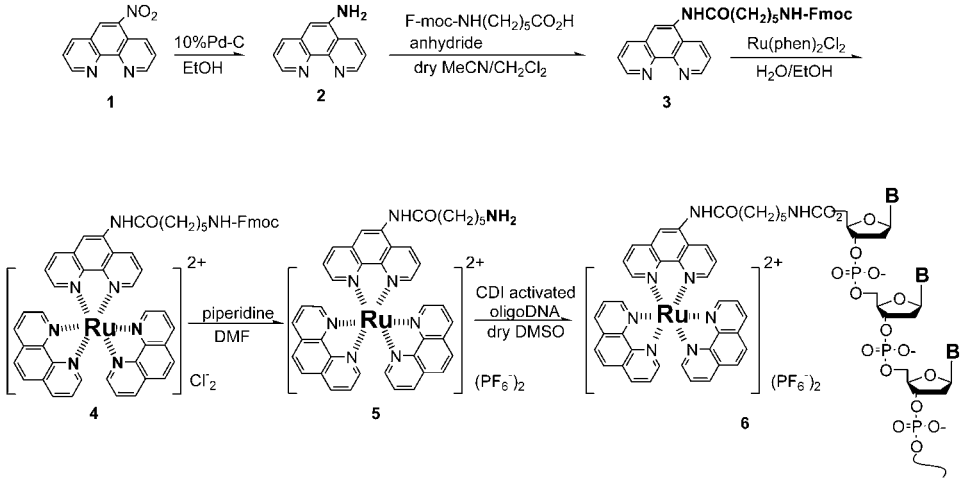

SCHEME 1

filtration, and the filtrate was evaporated to dryness. The residue was dissolved in piperidine/DMF (1:3 (v/v), 2 ml), and the solution was incubated at room temperature for 0.5 h. After evaporation, the residue was dissolved in MilliQ water (16 ml) and filtered. Then saturated NH_4PF_6 aqueous solution was added to the filtrate, and the orange precipitate that had formed was collected, yielding 0.10 g (95%).

Introduction of 5 to 5′ end of oligodeoxyribonucleotides

Oligodeoxyribonucleotides (ODN, 10 mer, Table 1) were synthesized according to general cyanoethyl phosphoramidite chemistry on a controlled pore glass support. The labeling reaction was carried out on the glass support in a filter-equipped air-tight syringe. The 5′ end of the ODN was activated by 1,1-carbonyldiimidazole (23), and bis-(1,10-phenanthroline) 5-(6-aminohexaneamide)-1,10-phenanthroline Ru(II) dihexafluorophosphate in dry dimethylsulfoxide (0.1 M) was added to the 1,1-carbonyldiimidazole-activated oligodeoxyribonucleotide on the glass support. After the incubation (60°C, 30 h), the glass support was washed sequentially with dimethylsulfoxide and acetonitrile. Deprotection of ODN and cleavage from the glass support were carried out according to conventional protocol. The crude solution of the Ru(II) complex-labeled ODN (Ru-probe) was purified by reverse-phase high-performance liquid chromatography with an acetonitrile gradient. Isomers of the Ru-probe were characterized by CD spectra.

Sample preparation and physical measurements

A solution of the 16S and 23S rRNA mixture (10 mM Tris-HCl (pH 7.5), 100 mM NaCl, and 1 mM $MgCl_2$) was incubated at 11°C for 24 h, and used for all sample preparations without further purification. The synthesized Ru-probe was dissolved in the same buffer solution as the rRNA and used for all sample preparations. All measurements were carried out at 11°C. The CD spectra were measured by a CD spectrophotometer (J-720, JASCO, Tokyo, Japan) equipped with a thermal controller (RET-100, Neslab, Portsmouth, NH). The melting temperatures of the hybrid of the Ru-probe and its complementary oligo-RNA were measured by a spectrophotometer (U-2000A, Hitach, Tokyo, Japan) equipped with a thermal controller. Luminescence anisotropy decay curves and emission decay curves were measured by a time-correlated single-photon counting system (NAES-550, Horiba, Kyoto, Japan) equipped with excitation (B390) and emission (Y52) filters and with a thermal controller. The luminescence spectra were measured by a spectrofluorophotometer (RF-5300PC, Shimadzu, Kyoto, Japan) equipped with a thermal controller.

TABLE 1 Sequences of Ru-probes and secondary structure of target site on 16S rRNA

	Target site	Structure around the target site	Sequence (5′ to 3′)
Ru-L1	L1 (887–896 nt)	internal loop	GCC GTA CTC C
Ru-L2	L2 (323–332 nt)	stem loop	CCG TGT CTC A
Ru-L3	L3 (557–566 nt)	internal loop	CAG TAA TTC C
Ru-L4	L4 (811–820 nt)	internal loop	ATC GTT TAC G
Ru-L5	L5 (1373–1382 nt)	internal loop	GAA CGT ATT C
Ru-L6	L6 (963–972 nt)	internal loop	GCG TTG CAT C
Ru-S1	S1 (634–643 nt)	stem	GTA TCA GAT G

THEORY

Time-resolved luminescence anisotropy measurement

The luminescence anisotropy decay curves ($r_{(t)}$) were calculated according to the following equation:

$$r_{(t)} = (I_{vv(t)} - G \times I_{vh(t)})/(I_{vv(t)} + 2 \times G \times I_{vh(t)}), \quad (1)$$

where the subscripts vv and vh of I indicate the orientation of the excitation and emission polarizers, respectively. For example, $I_{vv(t)}$ represents the intensity decay of the vertically polarized emission when excited by a vertically polarized light pulse. G, which is the instrumental responsive factor, was estimated from the following equation:

$$G = \sum_t I_{hv(t)} / \sum_t I_{hh(t)}. \quad (2)$$

From Eqs. 1 and 2, $r_{(t)}$ was obtained. The $r_{(t)}$ was fitted to the ideal curves represented by Eq. 3 using the nonlinear least-square deconvolution method

$$r_{(t)} = \sum_i r_{0i} \times (-t/\theta_i) + r_\infty, \quad (3)$$

where the r_{0i} are the fractional anisotropies that decay with the correlation time θ_i. The last term, r_∞, was used to account for the presence of a nonzero anisotropy at long time. From the fitted decay curve, the rotational correlation time (θ) was estimated. The predicted θ was calculated by the following equation:

$$\theta = \eta M w(h + \bar{v})/RT. \quad (4)$$

Evaluation of the Stern-Volmer constant

The emission intensity of the Ru-probe is represented by the following general Stern-Volmer equation:

$$I_{obs} = I_0/(1 + K_{sv} \times [Q]), \quad (5)$$

where I_{obs} and I_0 represent the observed emission intensity and the emission intensity in the absence of a quencher, respectively, and K_{sv} and $[Q]$ represent the Stern-Volmer constant and the concentration of the quencher in the medium, respectively. If hybridization occurs, it is assumed that two kinds of Ru-probe, i.e., free and bound probes, exist in the system. Based on this assumption, the emission intensity of the Ru-probe in the presence of 16S rRNA is represented by the following equation:

$$I_0/I = I_{0F}/I = I_{0F}/\{x \times [I_{0B}/(1 + K_{svB} \times [Q])] + (1 - x) \times [I_{0F}/(1 + K_{svF} \times [Q])]\}, \quad (6)$$

where I_{0F} and I_{0B} represent the emission intensity of the free and bound Ru-probes, respectively, K_{svF} and K_{svB} represent the Stern-Volmer constant of the free and bound Ru-probes, respectively, and x represents the binding ratio of the Ru-probe in the system. The titration curves of the quencher

molecule were fitted to Eq. 6. K_{svF} and K_{svB} were estimated from the fitted titration curves according to Eq. 6.

RESULTS AND DISCUSSION

To evaluate the rotational motion of biomolecules using time-resolved luminescence anisotropy analysis, the rotational correlation time, θ, is generally used as an indicator of the rotational motion. In our case, it was predicted that the θ value of the single-stranded regions of 16S rRNA was in the submicrosecond to microsecond range, according to Eq. 4. Therefore, to evaluate the segmental motions of the single-stranded regions of 16S rRNA, the lifetime of the luminescent probe needed to be around hundreds of nanoseconds. As a luminescent probe that could fulfill this requirement, we adopted the Ru(II) complex, the luminescence lifetime of which is ~500 ns to 1 μs. The Ru(II) complex was introduced to the 5′ end of ODN and used as a luminescent probe to evaluate the segmental motions of the single-stranded regions of 16S rRNA.

The oligonucleotide sequences of Ru-probes are summarized in Table 1. The target sites of 16S rRNA (1542 nt) were chosen on the basis of the reported secondary structure (24) (Fig. 1). The probes were purified by reverse-phase high-performance liquid chromatography, where the enantiomeric isomers (Δ and Λ isomers) were also isolated (20). The luminescence properties are summarized in Table 2. The difference in the luminescence properties between the enantiomers was negligible.

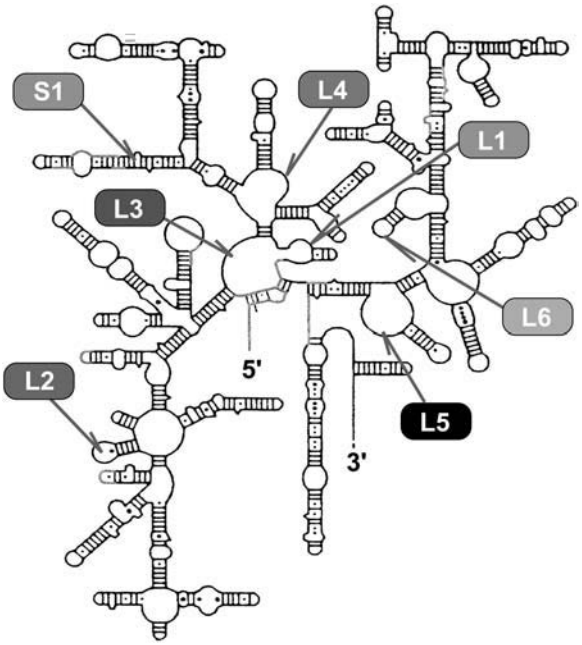

FIGURE 1 Reported secondary structure of *E. coli* 16S ribosomal RNA (24) and target sites of Ru-probes.

TABLE 2 Luminescence properties of Ru-probe

	$\lambda_{ex,max}$ (nm)	$\lambda_{em,max}$ (nm)	τ_1 (ns)	f_1	τ_2 (ns)	f_2	χ^2
Ru-probe Λ	461	587	1400	0.9	400	0.1	1.3
Ru-probe Δ	462	589	1300	0.8	100	0.2	1.4
$Ru(phen)_3^{2+}$	457	580	800	1	—	—	1.1

The oligonucleotide sequence of Ru probe is 5′ Ru-GCC GTA CTC C-3′. [Ru-probe] (or [$Ru(phen)_3^{2+}$]) = 0.75 μM in 10 mM Tris-HCl (pH 7.5) containing 100 mM NaCl and 1 mM $MgCl_2$. Measurements were carried out at 11°C.

It has been reported that Tris-1,10-phenanthroline Ru(II) complex ($Ru(phen)_3^{2+}$) interacts with double-helical DNA and that the luminescence intensity is enhanced by the interaction. It was also reported that the manner of the interaction differed for the different enantiomeric isomers of $Ru(phen)_3^{2+}$ (25). On the other hand, the binding affinity of the $Ru(phen)_3^{2+}$ to double-helical RNA was lower than that to double-helical DNA, and the enantioselectivity of the former interaction was negligible (25). Therefore, in this study, the Λ isomer was used as the luminescent probe. The emission spectrum of the Λ isomer of the Ru-probe was similar to that of $Ru(phen)_3^{2+}$, though the luminescence decay measurements showed the presence of two different lifetimes. The major component of the luminescence lifetime, τ_1, of the Ru-probe was longer than that of $Ru(phen)_3^{2+}$, suggesting that the oligonucleotide strand of the Ru-probe might interact with the $Ru(phen)_3^{2+}$ residue at the 5′ end of the oligonucleotide. As shown in Table 2, the τ_1 of the Ru-probe was long enough to evaluate the θ value of the single-stranded regions of 16S rRNA. The introduction of $Ru(phen)_3^{2+}$ to the oligodeoxyribonucleotide slightly changed the duplex stability (ΔT_m = −4–~2°C for the melting temperature estimated from the thermal denaturation curves).

To estimate the segmental motions of the single-stranded regions of 16S rRNA, the rotational correlation time (θ) of the Ru-probe/16S rRNA hybrid was measured. The anisotropy decay curves were well analyzed by a two-component exponential fitting, suggesting that there were two major luminescent species. The θ values calculated according to Eq. 3 are summarized in Table 3. The rotational correlation time, θ_2, was detected in several Ru-probes (Ru-L1, -L2, -L4,

TABLE 3 Time-resolved luminescence anisotropy analysis of Ru-probes in the presence of 16S rRNA

	θ_1 (ns)	r_{01}	θ_2 (ns)	r_{02}	r_∞	χ^2
Ru-L1 alone	9	0.06	n.d.	n.d.	n.d.	0.76
Ru-L1	6	0.09	1200	0.05	0.02	1.05
Ru-L2	18	0.03	150	0.04	0.01	1.27
Ru-L3	9	0.12	n.d.	n.d.	0.02	1.75
Ru-L4	8	0.07	590	0.05	n.d.	1.39
Ru-L5	29	0.08	380	0.01	0.05	1.10
Ru-L6	56	0.02	540	0.01	0.01	1.42
Ru-S1	22	0.11	n.d.	n.d.	n.d.	0.88

[Ru-probe] = [16S rRNA] = 0.75 μM in 10 mM Tris-HCl (pH 7.5) containing 100 mM NaCl and 1 mM $MgCl_2$. n.d., not detected.

-L5, and -L6) in the presence of 16S rRNA, whereas θ_2 was not detected in the case of the other Ru-probes (Ru-L3 and Ru-S1). This is probably due to the fact that the rotational motion of the Ru-probe was restricted and that the Ru-probe could hybridize with the single-stranded region of 16S rRNA. As the magnitude of θ_2 was different among the Ru-probes in the presence of 16S rRNA, it was suggested that each θ_2 represented the segmental motion of the single-stranded region of 16S rRNA on which the Ru-probes were hybridized. The order of magnitude of θ_2 suggested that the magnitude of the segmental motions of these sites were in the order L2 > L4 and L5 > L6 > L1. This order might provide information concerning flexibilities of the single-stranded regions of 16S rRNA in homogeneous physiological medium. That is, site L2 was the most flexible among the five sites. In almost all cases of the Ru-probes, a nonzero anisotropy at long time, r_∞, was observed in the presence of 16S rRNA. This observation is the result of the presence of slow motion(s) that display long θ(s) which cannot be observed with 0.5–~1 μs luminescence decay time Ru-probe.

To further characterize the single-stranded regions of 16S rRNA in which the Ru-probes were hybridized, the luminescence lifetimes of the Ru-probes were measured (Table 4). Three cases in which the luminescence lifetime of $Ru(phen)_3^{2+}$ increased have been reported. They are the cases when 1), the Ru complex is intercalated with the double-helical DNA (26), 2), the Ru(II) complex is isolated from quencher molecules such as solvents or salts, and 3), the Ru(II) complex is located in a high-ionic-strength environment. In all cases, it was assumed that the luminescence lifetimes of the Ru-probes that were bound to their target sites were largely concerned with the entangling of the RNA strand around the single-stranded regions of 16S rRNA where the Ru-probes hybridized. In our case, the addition of 16S rRNA caused a remarkable increase of the luminescence lifetime of Ru-L1 compared with the other Ru-probes. This result indicated at least that the entangling of the RNA strand around the L1 site was relatively high. That is, the local nucleotide density around L1 might be relatively high compared with the other sites chosen, which made sense based on the flexibility of L1.

To verify this assumption, a luminescence quenching study was performed. As a quencher molecule, potassium ferrocyanide ($K_4[Fe(CN)_6]$), which is a good quencher of Ru(II) complex derivatives (25), was adopted. Potassium ferrocyanide was added to the mixture of the Ru-probe and 16S rRNA, and the luminescence intensity was measured in the presence of various concentrations of ferrocyanide anion (Fig. 2). The resulting Stern-Volmer constants (K_{sv}) of the derivatives of the Ru(II) complex are summarized in Table 5. The K_{sv}s of the Ru-probes were lower than that of $Ru(phen)_3^{2+}$. This result suggested that the oligonucleotide strand of the Ru-probe might inhibit the access of the ferrocyanide anion to the Ru(II) complex. $K_{sv\ B}$ was detected by the addition of 16S rRNA, indicating that the binding of the Ru-probes to 16S rRNA inhibited the access of the ferrocyanide anion to the Ru(II) complexes conjugated with the oligonucleotides. The difference in $K_{sv\ B}$ of Ru-L1 and -L2 in the presence of 16S rRNA indicated that the environments around the bound Ru-probes were different between these two Ru-probes. That is, the collision frequencies of ferrocyanide anion to the Ru(II) complexes were quite different. It was assumed that the Ru(II)

TABLE 4 Luminescence lifetimes of Ru-probes in the presence or absence of 16S rRNA

	τ_1 (ns)	f_1	τ_2 (ns)	f_2	χ^2
Ru-L1	1350 (10)*	0.91	400 (70)*	0.09	1.30
+ rRNA	1690 (20)	0.80	550 (50)	0.20	1.03
Ru-L2	1300 (<10)	0.86	210 (30)	0.14	1.22
+ rRNA	1380 (10)	0.85	360 (40)	0.15	1.32
Ru-L3	1170 (<10)	0.85	60 (10)	0.15	1.54
+ rRNA	1260 (<10)	0.86	240 (30)	0.14	1.42
Ru-L4	1120 (<10)	0.84	180 (10)	0.16	1.35
+ rRNA	1270 (10)	0.82	360 (30)	0.18	1.66
Ru-L5	1210 (<10)	0.89	100 (20)	0.11	1.63
+ rRNA	1230 (<10)	0.84	280 (20)	0.16	1.64
Ru-L6	1350 (<10)	0.86	240 (20)	0.14	1.12
+ rRNA	1330 (<10)	0.84	230 (20)	0.16	1.56
Ru-S1	1300 (<10)	0.86	210 (30)	0.14	1.22
+ rRNA	1380 (10)	0.85	360 (40)	0.15	1.32

[Ru-probe] = [16S rRNA] = 0.75 μM in 10 mM Tris-HCl (pH 7.5) containing 100 mM NaCl and 1 mM $MgCl_2$. Values in parentheses indicate asymptotic standard errors.

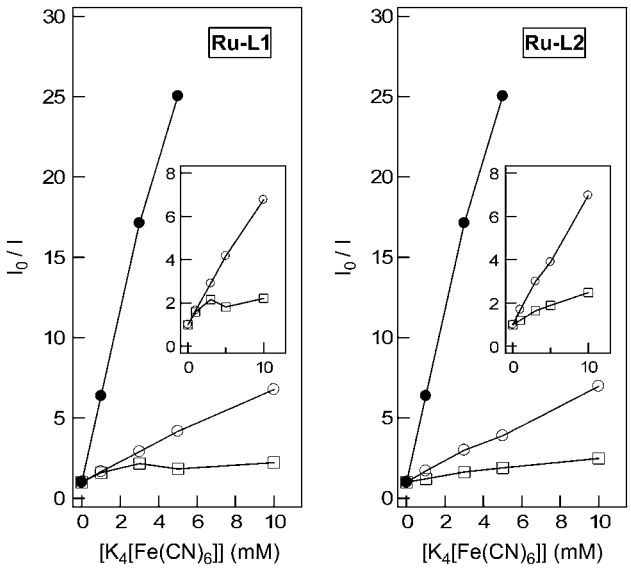

FIGURE 2 Stern-Volmer plot of the emission from Ru-probe in the presence or absence of 16S rRNA. Solid circles represent the profile of $[Ru(phen)_3]Cl_2$. Open circles and squares represent the profiles of the Ru-probe in the absence and presence, respectively, of 16S rRNA. [Ru derivative] = 0.75 μM in 10 mM Tris-HCl buffer (pH 7.5) containing 100 mM NaCl and 1 mM $MgCl_2$. The excitation wavelength was 453 nm with observation at 583 nm and a bandpass of 5 nm at 11°C.

TABLE 5 Stern-Volmer constant (K_{sv}) of Ru-probes in the presence or absence of 16S rRNA

	$K_{sv\ F}$ (M^{-1})*	$K_{sv\ B}$ (M^{-1})*	Bound ratio
Ru-L1	576	—	—
+ rRNA	576	61	0.61
Ru-L2	589	—	—
+ rRNA	589	94	0.56
$Ru(phen)_3^{2+}$	4850	—	—

*K_{sv} was estimated from Fig. 2 by the curve-fitting protocol according to Eq. 6.

complex of Ru-L2 located around its target site underwent frequent collision by ferrocyanide anion, whereas that of Ru-L1 did not. This result was in good agreement with the flexibilities of these single-stranded regions, as already discussed.

Based on the results discussed above, we proposed a novel concept for predicting the local flexibility of the single-stranded regions, which significantly affects their interaction with other biomolecules. To further verify this proposal, the flexibilities of the single-stranded regions were evaluated from the viewpoint of hybridization kinetics. We previously reported the kinetics of interactions between single-stranded regions of 16S rRNA and their complementary oligonucleotides by fluorescence anisotropy analysis using 5′-fluorescein-labeled oligonucleotides (27). In the report, we concluded that the L2 site accepted its complementary oligonucleotide far more rapidly than did the L1 site. The order of magnitude of the association rate constant (k_{assoc}) and dissociation rate constant (k_{dissoc}) of the hybridization was L2 > L6 > L1. This result suggested that a rapidly moving site, like L2, rather promptly accepts its complementary oligonucleotide, whereas a slowly moving site, like L1, reluctantly accepts its complementary oligonucleotide.

Taking these results into consideration, it seems that the L1 site was located in the depths of the 16S rRNA, and that the L2 site was on the relatively outer region of 16S rRNA. Such information is of great importance in the designing of RNA-acting molecules. Some molecules might interact with the stem regions and some with the single-stranded ones. Antisense molecules, especially, have to hybridize with the latter regions. Static analysis using a steady-state fluorescence method clearly predicted the single-stranded regions in the folded RNA (28). However, static information is not enough when designing antisense molecules (29). If the regions are located deep in the RNA, the antisense molecule may take time to reach the region and to hybridize with it. By that time, in the competition with cellular processes such as translocation of ribosome, the antisense effect could be diminished. If the regions are located in the surface of RNA, the antisense molecules can easily hybridize with the region, and there, RNase H can promptly recognize the heteroduplex. The static analysis is quite ineffective for such evaluation, and only time-resolved luminescence anisotropy analysis using a long-lifetime luminescent probe is effective for the purpose.

In conclusion, the segmental motions of single-stranded regions of 16S rRNA were estimated by the time-resolved luminescence anisotropy analysis using a long-lifetime Ru(II) complex-labeled oligonucleotide as a probe. Results from the luminescence lifetime and luminescence quenching experiments were in good agreement with the prediction from the measurement of the segmental motions. It was predicted that the segmental motion, namely flexibility, is correlated to the depth from the surface of the 16S rRNA. Comparison between the flexibility of the single-stranded regions and the hybridization kinetics with their complementary oligonucleotides suggested a significant correlation between the flexibility and hybridization kinetics.

This research was partly supported by the Kyoto Nanotechnology Cluster of the Knowledge Cluster Initiative administrated by the Ministry of Education, Science, Sports and Culture of Japan. Support from Otsuka GEN Research Institute, administrated by Otsuka Pharmaceutical, is gratefully acknowledged.

REFERENCES

1. Ban, N., P. Nissen, J. Hansen, P. B. Moore, and T. A. Steitz. 2000. The complete atomic structure of the large ribosomal subunit at 2.4 Å resolution. *Science*. 289:905–920.
2. Clemons, W. M., Jr., J. L. May, B. T. Wimberly, J. P. McCutcheon, M. S. Capel, and V. Ramakrishnan. 1999. Structure of a bacterial 30S ribosomal subunit at 5.5 Å resolution. *Nature*. 400:833–840.
3. Carter, A. P., W. M. Clemons, D. E. Brodersen, R. J. Morgan-Warren, B. T. Wimberly, and V. Ramakrishnan. 2000. Functional insights from the structure of the 30S ribosomal subunit and its interactions with antibiotics. *Nature*. 407:340–348.
4. Augusteyn, R. C. 2004. α-crystallin: a review of its structure and function. *Clin. Exp. Optom.* 87:356–366.
5. Manley, P. W., G. Bold, J. Bruggen, G. Fendrich, P. Furet, J. Mestan, C. Schnell, B. Stolz, T. Meyer, B. Meyhack, W. Stark, A. Strauss, and J. Wood. 2004. Advances in the structural biology, design and clinical development of VEGF-R kinase inhibitors for the treatment of angiogenesis. *Biochim. Biophys. Acta*. 1697:17–27.
6. Bechinger, B., C. Aisenbrey, and P. Bertani. 2004. The alignment, structure and dynamics of membrane-associated polypeptides by solid-state NMR spectroscopy. *Biochim. Biophys. Acta*. 1666:190–204.
7. Tamm, L. K., F. Abildgaard, A. Arora, H. Blad, and J. H. Bushweller. 2003. Structure, dynamics and function of the outer membrane protein A (OmpA) and influenza hemagglutinin fusion domain in detergent micelles by solution NMR. *FEBS Lett.* 555:139–143.
8. Jao, C. C., A. Der-Sarkissian, J. Chen, and R. Langen. 2004. Structure of membrane-bound α-synuclein studied by site-directed spin labeling. *Proc. Natl. Acad. Sci. USA*. 101:8331–8336.
9. Isas, J. M., R. Langen, W. L. Hubbell, and H. T. Haigler. 2004. Structure and dynamics of a helical hairpin that mediates calcium-dependent membrane binding of annexin B12. *J. Biol. Chem.* 279: 32492–32498.
10. Tuschl, T., C. Gohlke, T. M. Jovin, E. Westhof, and F. Eckstein. 1994. A three-dimensional model for the hammerhead ribozyme based on fluorescence measurements. *Science*. 266:785–789.
11. Silverman, S. K., and T. R. Cech. 1999. RNA tertiary folding monitored by fluorescence of covalently attached pyrene. *Biochemistry*. 38: 14224–14237.

12. McCord, E. F., K. M. Morden, I. Tinoco, Jr., and S. G. Boxer. 1984. Chemically induced dynamic nuclear polarization studies of yeast tRNAPhe. *Biochemistry.* 23:1935–1939.

13. Roberts, M. F., Q. Cui, C. J. Turner, D. A. Case, and A. G. Redfield. 2004. High-resolution field-cycling NMR studies of a DNA octamer as a probe of phosphodiester dynamics and comparison with computer simulation. *Biochemistry.* 43:3637–3650.

14. Finerty, P. J., Jr., A. K. Mittermaier, R. Muhandiram, L. E. Kay, and J. D. Forman-Kay. 2005. NMR dynamics-derived insights into the binding properties of a peptide interacting with an SH2 domain. *Biochemistry.* 44:694–703.

15. Okonogi, T. M., A. W. Reese, S. C. Alley, P. B. Hopkins, and B. H. Robinson. 1999. Flexibility of duplex DNA on the submicrosecond timescale. *Biophys. J.* 77:3256–3276.

16. Simon-Lukasik, K. V., A. V. Persikov, B. Brodsky, J. A. Ramshaw, W. R. Laws, J. B. Alexander Ross, and R. D. Ludescher. 2003. Fluorescence determination of tryptophan side-chain accessibility and dynamics in triple-helical collagen-like peptides. *Biophys. J.* 84:501–508.

17. Lakowicz, J. R. 1999. Principles of Fluorescence Spectroscopy, 2nd ed. Kluwer Academic/Plenum Publishers, New York.

18. Hartshorn, R. M., and J. K. Barton. 1992. Novel dipyridophenazine complexes of Ruthenium(II): exploring luminescent reporters of DNA *J. Am. Chem. Soc.* 114:5919–5925.

19. Milton, R. C., E. Becker, S. C. Milton, J. E. Baxter, and J. F. Elsworth. 1987. Improved purities for Fmoc-amino acids from Fmoc-ONSu. *Int. J. Pept. Protein Res.* 30:431–432.

20. Meggers, E., D. Kusch, and B. Giese. 1997. An efficient synthesis of enantiomerically pure delta- and lambda-Ruthenium(II)-labeled oligonucleotides. *Helv. Chimica Acta.* 80:640–652.

21. Sullivan, B. P., D. J. Salmon, and T. J. Meyer. 1978. Mixed phosphine 2,2′-bipyridine complexes of ruthenium. *Inorg. Chem.* 17:3334–3341.

22. Terpetschnig, E., H. Szmacinski, and J. R. Lakowicz. 1995. Fluorescence polarization immunoassay of a high-molecular-weight antigen based on a long-lifetime Ru-ligand complex. *Anal. Biochem.* 227:140–147.

23. Wachter, L., J. A. Jablonski, and K. L. Ramachandran. 1986. A simple and efficient procedure for the synthesis of 5′-aminoalkyl oligodeoxynucleotides. *Nucleic Acids Res.* 14:7985–7994.

24. Gutell, R. R., N. Larsen, and C. R. Woese. 1994. Lessons from an evolving rRNA: 16S and 23S rRNA structures from a comparative perspective. *Microbiol. Rev.* 58:10–26.

25. Barton, J. K., J. M. Goldberg, C. V. Kumar, and N. J. Turro. 1986. Binding modes and base specificity of Tris(phenanthroline)ruthenium(II) enantiomers with nucleic acids: tuning the stereoselectivity. *J. Am. Chem. Soc.* 108:2081–2082.

26. Kumar, C. V., J. K. Barton, and N. J. Turro. 1985. Photophysics of Ruthenium complexes bound to double helical DNA. *J. Am. Chem. Soc.* 107:5518–5523.

27. Sakamoto, T., A. Mahara, R. Iwase, T. Yamaoka, and A. Murakami. 2005. Analytical method for estimation of kinetics of oligonucleotide/RNA hybridization using fluorescence depolarization spectroscopy. *Anal. Biochem.* 340:369–372.

28. Mahara, A., R. Iwase, T. Sakamoto, T. Yamaoka, K. Yamana, and A. Murakami. 2003. Detection of acceptor sites for antisense oligonucleotides on native folded RNA by fluorescence spectroscopy. *Bioorg. Med. Chem.* 11:2783–2790.

29. Wang, J.-Y., and K. Drlica. 2004. Computational identification of antisense oligonucleotides that rapidly hybridize to RNA. *Oligonucleotides.* 14:167–175.